PAPER

Low-temperature electrolytes based on linear carboxylic ester co-solvents for SiOx/graphite composite anodes†

Rui Wang,[a] Jingwen Cao,[a] Chunyu Xu,[a] Ningning Wu,[a] Shu Zhang [iD] *[ab] and Mengqiang Wu [iD] *[ab]

Silicon-based anode materials have been applied in lithium-ion batteries with high energy density. However, developing electrolytes that can meet the specific requirements of these batteries at low temperatures still remains a challenge. Herein, we report the effect of linear carboxylic ester ethyl propionate (EP), as the co-solvent in a carbonate-based electrolyte, on SiOx/graphite (SiOC) composite anodes. Using electrolytes with EP, the anode provides better electrochemical performance at both low temperatures and ambient temperature, showing a capacity of 680.31 mA h g^{-1} at -50 °C and 0.1C (63.66% retention relative to that at 25 °C), and a capacity retention of 97.02% after 100 cycles at 25 °C and 0.5C. Within the EP-containing electrolyte, SiOC‖LiCoO$_2$ full cells also exhibit superior cycling stability at -20 °C for 200 cycles. These substantial improvements of the EP co-solvent at low temperatures are probably due to its involvement to form a solid electrolyte interphase with high integrity and facile transport kinetics in electrochemical processes.

1. Introduction

The application of SiOx/graphite composite anodes boosts the development and commercialization of lithium-ion batteries (LIBs) with high energy density and low cost.[1–7] However, the poor performance of SiOx/graphite-based LIBs at low temperatures severely hampered their large-scale applications. As an indispensable component in LIBs, the electrolyte plays a significant role in improving the low-temperature performance of SiOx/graphite-based LIBs. For instance, to address the issues of large volume fluctuation during cycling and fragile solid electrolyte interphase (SEI) associated with SiOx/graphite electrodes, researchers have carried out intensive studies to understand the correlation of electrolyte formulation with the stability and integrity of SEI at low temperatures.[8–18]

Designing and regulating the electrolyte formulation by adjusting co-solvents is a straightforward and efficient strategy to optimize the properties of LIBs for special requirements.[19–22] For LIBs applied in a low temperature scenario, linear carboxylates, with low melting points and viscosities, are commonly used as co-solvents to achieve higher conductivity of electrolytes

and improved mobility of Li$^+$ ions.[23–27] Specifically, ethyl propionate (EP), having a melting point of -73 °C and a boiling point of 99 °C, has been widely used in electrolytes for low-temperature LIBs.[23] For instance, the addition of EP to carbonate-based electrolytes can facilitate the intercalation/de-intercalation kinetics of Li$^+$ in MCMB‖LiNi$_{0.8}$Co$_{0.2}$O$_2$ cells. Such promotion effect also reflected in the improvement of electrochemical performance at -60 °C.[25] Similarly,[24] EP guarantees a higher conductivity of electrolytes at low temperatures thanks to its low viscosity and melting point. Thus, the charge transfer resistance (R_{ct}) of graphite‖LiMn$_2$O$_4$ cell is effectively reduced and the cell can withstand a discharge current of 5C at -20 °C with a capacity retention of 93%. Although current studies are focused on the enhancement for graphite anodes, the effect of ester co-solvents on the electrolyte matching with SiOx/graphite (SiOC) anodes remains yet to be elucidated. Furthermore, it is challenging to exploit the low-temperature electrolyte highly suitable for silicon-based anodes.

The goal of this study is to understand the influence of ester co-solvents on the electrochemical performance of Si-based anodes and to develop low-temperature electrolytes for these anodes. Herein, we chose EP as the representative ester co-solvent and compared the electrochemical performance of a SiOC composite anode, including low-temperature specific capacity and cycling stability, using conventional carbonate-based electrolytes with and without EP co-solvents. With the electrolyte containing EP, the SiOC anode showed a high charging capacity of 680.31 mA h g^{-1} with an excellent capacity retention of 63.66% at -50 °C. Furthermore, SiOC‖LCO full

[a]School of Materials and Energy, University of Electronic Science and Technology of China, 2006 Xiyuan Avenue, West High-Tech Zone, Chengdu 611731, China. E-mail: shuzhang@uestc.edu.cn; mwu@uestc.edu.cn

[b]The Yangtze Delta Region Institute (Huzhou), University of Electronic Science and Technology of China, Huzhou 313001, China

† Electronic supplementary information (ESI) available. See DOI: https://doi.org/10.1039/d3ra01111a

RSC Advances

cells using this electrolyte showed stable charge–discharge cycling at −20 °C and 0.1C, with an average discharge capacity of 385.86 mA h g^{-1} (based on the mass of the SiOC material) for 200 cycles. SEM, TEM and XPS results collectively indicate that EP plays an important role in the formation of LiF-rich SEI with ductility on the surface of the SiOC anode, which subsequently resists the volume fluctuation of the silicon-based anode during charge–discharge tests. This work provides an efficient method for improving the low-temperature performance of silicon-based anodes.

2. Experimental

2.1. Materials

SiOC powder was purchased from Shanghai Yuling New Energy Technology Co., Ltd. A SONE binder was supplied by Shenzhen Kejing Zhida Technology Co., Ltd. Ethylene carbonate (EC), propylene carbonate (PC), fluoroethylene carbonate (FEC), diethyl carbonate (DEC), ethyl propanoate (EP), and lithium hexafluorophosphate (LiPF$_6$) were all obtained from DoDo Chemical Technology Co., Ltd.

2.2. Electrolyte preparation

The preparation of the two electrolytes was carried out in an argon-filled glove box with less than 0.1 ppm water and less than 0.5 ppm oxygen. The compositions of the two electrolytes are listed in Table 1 and, for clarity, are denoted as E1 and E2.

2.3. Electrode fabrication and cell assembly

SiOC and the SONE binder with a weight ratio of 90 : 10 were ground together for 30 min, coated (with a thickness of 100 μm) on the rough side of a copper foil, dried in a vacuum oven at 70 °C for 12 h and then cut into circular pieces of 14 mm diameter (1.54 cm^2) with a mass loading of active material between 1.64 and 1.77 mg cm^{-2}. Since the SONE binder itself contains carbon nanotubes, no additional conductive agent is needed. A LCO electrode was fabricated by a similar method. LCO powder, Super P and polyvinylidene difluoride (PVDF) with a weight ratio of 90 : 5 : 5 were ground with 1-methyl-2-pyrrolidinone (NMP) for 30 min to prepare a LCO slurry, which was then coated (with a thickness of 250 μm) onto an aluminum foil. The mass loading of the LCO active material on the electrode is between 9.47 and 9.85 mg cm^{-2}. The half cell and full cell were assembled and sealed in a glove box, using Celgard 2400 as the separator in CR2032 coin-type cases with 50 μL electrolyte for each cell.

2.4. Electrochemical tests

A charging/discharging test was performed using a Neware battery test system (CT-4008T, Shenzhen, China). The charge/discharge cutoff voltage is 5 mV/2 V, and the C-rate setting is based on the specific capacity of 1000 mA h g^{-1} of SiOC active material. Before every electrochemical test, cells were first cycled at 25 °C and 0.05C for three cycles, and for low-temperature tests, extra 10 cycles at 0.1C were added to enable the formation of stable SEI. The performance at low temperatures was carried out in a low-temperature oven (MSK-TE906, Shenzhen, China) before cells were left at the setting temperature for one hour to reach thermal equilibrium. The electrochemical impedance spectroscopy (EIS) data, the cyclic voltammetry (CV) data and the linear sweep voltammetry (LSV) data were obtained using an electrochemical workstation (Chenhua CHI660E, Shanghai, China). The ionic conductivity tests at target low temperatures were performed using a Leici conductivity tester (DDS-307, Shanghai, China).

2.5. Characterization

The tested cells were carefully disassembled in the glove box, and the resulting electrodes were soaked with a dimethyl carbonate (DMC) solution to remove the redundant electrolyte on the surface. The surface morphology images and the energy-dispersive spectroscopy (EDS) elemental mapping of electrodes were acquired using scanning electron microscopy (SEM, JSM-7500F, JEOL) and transmission electron microscopy (TEM, Tecnai G2 F20 S-TWIN, FEI). The surface composition change of electrodes was characterized by X-ray photoelectron spectroscopy (XPS, Thermo Scientific K-Alpha+). X-ray diffraction (XRD) patterns of the SiOC electrode were obtained using an X-ray powder diffractometer (UltimalV). Thermogravimetric analysis (TGA) was carried out using a TGA/DSC1 STARe system with a continuous O$_2$ flow in the temperature range of 0–1000 °C to determine the content of carbon. Raman spectroscopy was performed using a Horiba scientific instrument to analyze the solvation structure of the two electrolytes in the range of 250–2000 cm^{-1} at an excitation wavelength of 532 nm.

3. Results and discussion

The SiOC composite material, as the Si-based anode material in this study, was characterized by several techniques, as shown in Fig. 1. The XRD pattern of SiOC (Fig. 1a) showed a narrow and distinct peak at 26.38° that was indexed as a typical graphite peak. The enlarged peaks in the range of 20–25° corresponded to non-stoichiometry SiO$_x$ and the residual diffraction peaks could be assigned to small amounts of Si and SiO$_2$, which were the starting materials for the preparation of SiO$_x$.[28–30] The

Table 1 Electrolyte formulations in this study

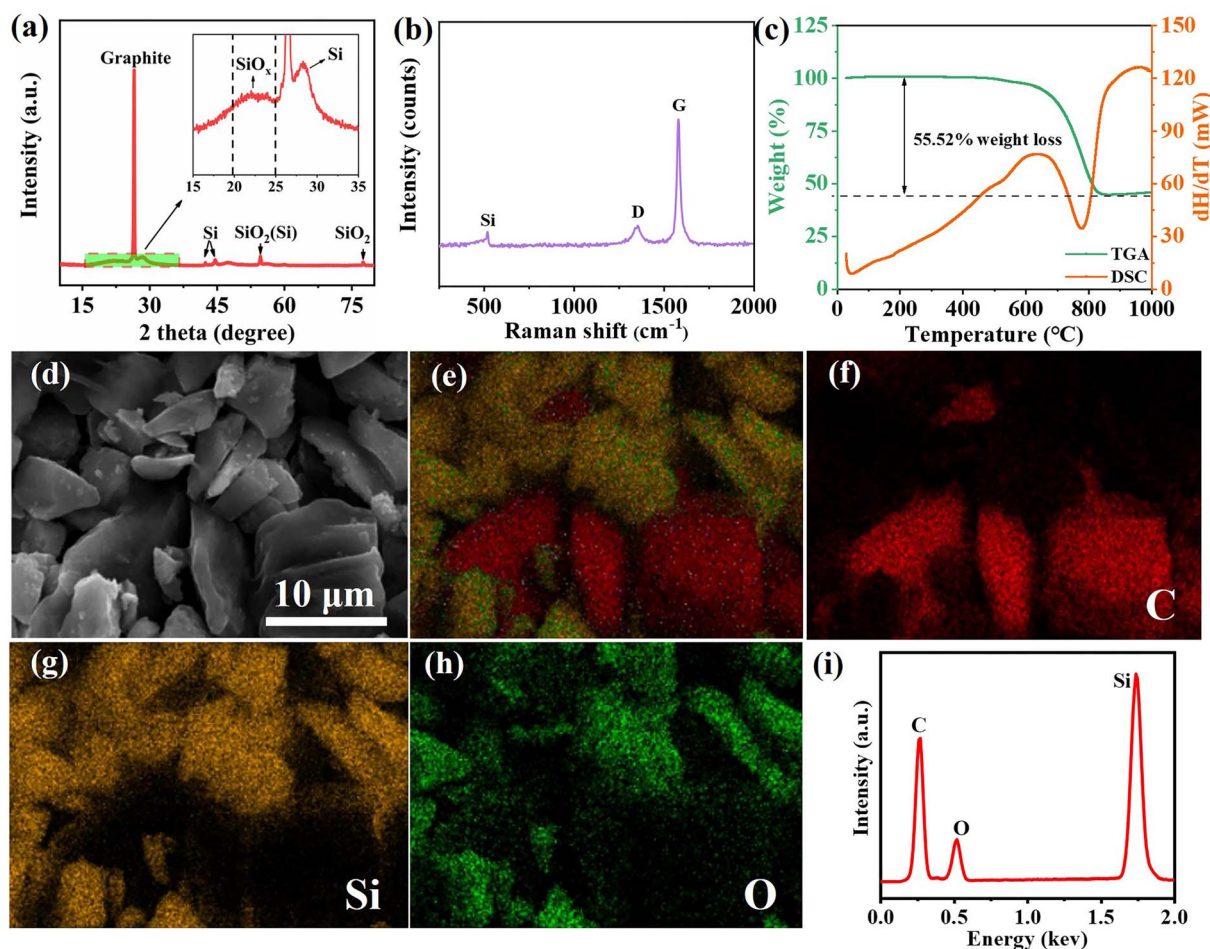| Electrolyte	Formation
E1	1.2 M LiPF$_6$ in DEC–PC–EC–FEC (20:1:4:2 by volume)
E2	1.2 M LiPF$_6$ in DEC–EP–PC–EC–FEC (10:10:1:4:2 by volume)

Fig. 1 Characterization of the SiOC starting material: (a) XRD pattern; (b) Raman spectrum; (c) TGA and DSC curves; (d) SEM image of the pristine electrode; (e–i) EDS elemental mapping images and EDS spectrum of the pristine electrode.

Raman spectrum of SiOC (Fig. 1b) also confirmed the existence of crystalline Si (with a vibration band at 520.56 cm^{-1}) and graphite (with a D peak at 1355.92 cm^{-1} and a G peak at 1576.28 cm^{-1}).[31] The integrated intensity ratio I_D/I_G of 0.32 indicated a relatively high degree of disorder for the graphite. The carbon content in SiOC was determined by TGA (Fig. 1c), corresponding to a weight loss of 55.52% in the range of 610–820 °C as oxidation of carbon. Fig. 1d–i show the SEM and EDS elemental mapping images of the pristine SiOC electrode. These images verified that the active material was a mixture of graphite and SiO$_x$ with a similar particle size of about 5 μm.

In this study, we designed two electrolytes, E1 and E2, using the formula provided in Table 1. Both electrolytes contained 1.2 M LiPF$_6$, and in E1 half (by volume) of the DEC linear carbonate component was replaced with linear carbonylic ester EP. We chose EP as the ester co-solvent because its low melting point (−75 °C) and low viscosity (0.502 cP, 25 °C) are suitable for low-temperature electrolytes.[32] The physical properties of the two electrolytes were also characterized. Both electrolytes remained liquid at −60 °C, showing the possibility for application at low temperatures (Fig. 2b). The effect of EP on the SiOC anode was analyzed by the theoretical calculation (Fig. 2a).

The energy level of the lowest unoccupied molecular orbital (LUMO) for EP (0.28 eV) is lower than these of DEC (0.92 eV), EC (0.63 eV), FEC (0.31 eV) and PC (0.63 eV), indicating that EP may be first reduced on the anode surface and involved in the formation of SEI.[33] Electrostatic potential maps (EPMs) of EP displayed in Fig. 2c show that the negative region of EP is centered on the carbonyl O atom, and thus, it is the favorable site for binding to Li$^+$ cations during solvation.[34] The LSV and CV results presented in Fig. S1† reveal that both electrolytes possess reliable oxidation stability within the target voltage range.

In Fig. 2d, although the measured ionic conductivity drops sharply as the temperature decreases, E2 offers superior ionic conductivity relative to E1, even at a temperature as low as −60 °C, because EP reduces the viscosity and freezing point of electrolyte E2 at low temperatures. Reliable ionic conductivity is one prerequisite for excellent electrochemical performances at low temperatures, as demonstrated previously.[24]

Fig. 3a and b show the charge curves of SiOC half cells with E1 and E2 electrolytes, respectively, at different temperatures of −60 to 25 °C. The capacity of SiOC using E2 at 25 °C is 1069.15 mA h g^{-1}, which is 82.06 mA h g^{-1} higher than that of

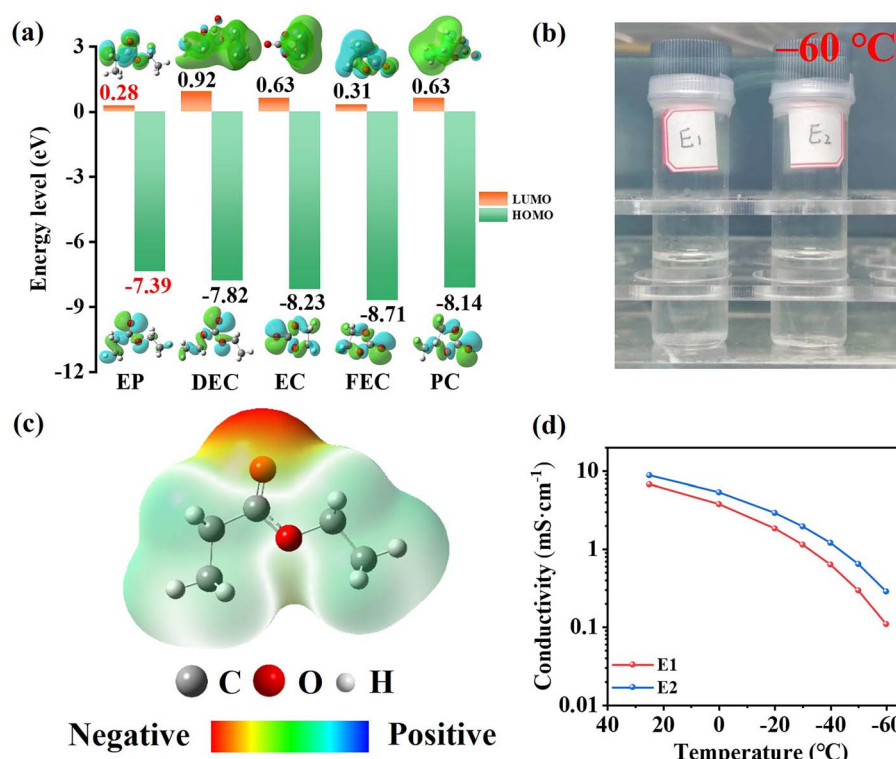**Fig. 2** (a) Theoretical calculation of the LUMO and HOMO energy level of EP, DEC, EC, FEC and PC molecules. (b) E1 and E2 remain liquid at −60 °C. (c) Electrostatic potential maps (EPM) of EP. (d) Ionic conductivity−temperature curves of E1 and E2.

E1. For half cells with both electrolytes, as the temperature decreases, the onset of the charge potential increases along with the loss of charge capacity. Comparing the capacity retention in Fig. 3c, more pronounced capacity retention is observed for SiOC using E2 as the temperature declined. For instance, at −50 °C, the capacity retention in E2 is still 63.66% of the maximum value at 25 °C, nearly 1.5 times higher than that in E1 (39.21%). The better capacity retention for SiOC in E2 can be ascribed to the much lower viscosity and melting point of EP co-solvent.[27]

Other than subzero performance, SiOC with the E2 electrolyte shows improved cycling stability and rate performance at 25 °C relative to that with E1 (Fig. 3d). The specific capacity with E1 decays rapidly from 811.62 mA h g^{-1} to 650.01 mA h g^{-1} in the first 10 cycles and then rises gradually, consistent with the reported performance of silicon-based anodes.[35–37] The initial decay of capacity originates from repeating volume expansion of SiO$_x$ particles and SEI fracture, in which process an increasing number of Si active sites are exposed to store lithium, contributing to the later augment of capacity.[38] Meanwhile, the effective lithiation-induced reactivation process makes the SEI stable, and subsequently, has positive effects on capacity delivery.[39] In contrast, SiOC provides an initial specific capacity of 863.70 mA h g^{-1} in E2, and with a slight drop to 799.11 mA h g^{-1}, is then stabilized at 900.00 mA h g^{-1} with an average excellent coulombic efficiency of 99.60% for about 100 cycles. This different electrochemical behavior indicates that EP in E2 is probably involved in the initial SEI formation to

stabilize the following cycle process. By comparing the charge–discharge curves in Fig. 3e and f, the superior cycling stability of the SiOC material in E2 was further verified. To further examine the kinetic property of the SiOC material in the two different electrolytes,[40,41] we compared the rate performance of half cells at 25 °C (Fig. 3g–i). The reversible capacities of E2 at rates of 0.1, 0.2 0.5, 1, and 2C are 1011.44, 951.79, 779.08, 580.92, and 427.22 mA h g^{-1}, respectively. For these measured rates, cells using E2 always achieve more stable cycles with a higher capacity than cells using E1. EIS comparison (Fig. S2†) shows more than twice of charge transfer resistance (R_{ct}) for cells in E1 than these in E2 at all tested temperatures. Collectively, all results indicate that EP plays an important role in optimizing the electrochemical performance of the SiOC anode material, at low temperatures and ambient temperature, through the change of SEI formation for SiOC and effective decreased R_{ct} in the cell.[42]

The morphologies of electrodes at different cycles were determined by SEM. Fig. 4a and d exhibit the surface morphology of electrodes with E1 and E2, respectively, after one cycle at 0.1C and 25 °C. Various unevenly distributed fine particles grow on the surface of the SiOC electrode using E1, revealing that the formation of SEI is inhomogeneous in E1 at the initial cycle. In comparison, smooth and homogenous SEI covers the surface of the active material with E2, indicating better SEI-formation ability of E2 on the SiOC anode. After 10 cycles at 0.1C, the SiOC powder with E1 ruptures (Fig. 4b); a long and obvious crack appears and the fresh active material is
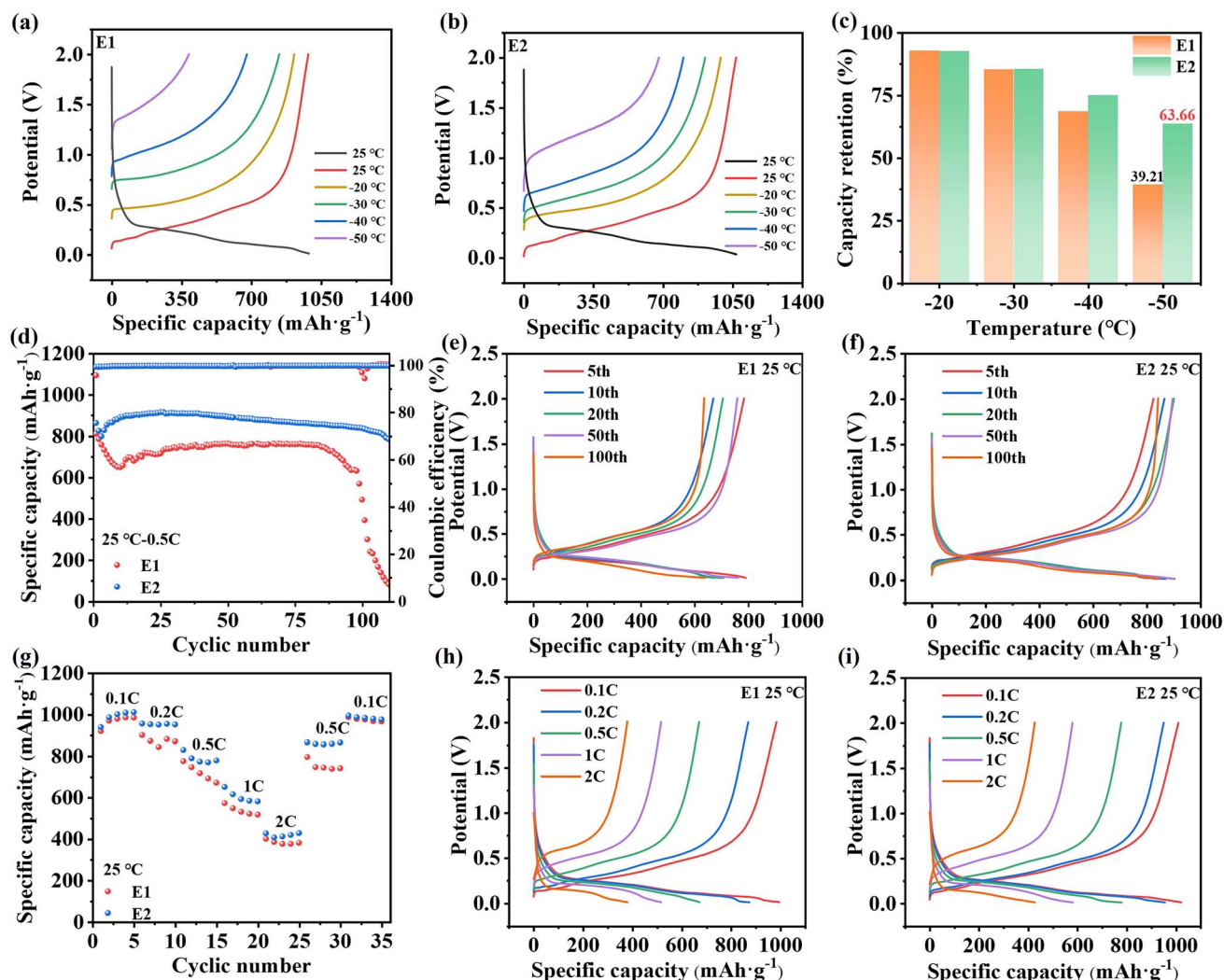
Fig. 3 Comparison of electrochemical performance of SiOC half cells with E1 and E2 electrolytes: charge curves at 0.1C at different temperatures with (a) E1, (b) E2 electrolytes, and (c) capacity retention; specific capacity at 0.5C at 25 °C: (d) cyclic performance, and corresponding charge–discharge curves with (e) E1 and (f) E2 for selected cycles. (g) Rate performance at 25 °C and corresponding charge–discharge curves with (h) E1 and (i) E2 of different rates.

exposed, which will further consume electrolyte and reversible Li$^+$ ions in cycling. On the surface of SiOC using E2 (Fig. 4e), although thick surface layers still appear, particles of the active material remain intact and the original SEI seems compatible with the expanded volume and inhibits the shedding and pulverization of SiOC in the electrochemical process. After charging at low temperatures, the uneven accumulation of particles occurred at the cracks of E1 (Fig. 4c), and the nonuniform distribution of particles may be relevant to the unexpected viscosity, low ionic conductivity and poor infiltration of E1 at low temperatures. However, with the existence of EP, SiOC maintains its original morphology even at low temperatures (Fig. 4f), and the particles grow closely on the surface and the particle size is uniform. As shown in Fig. S3,† this difference is also obvious on a large scale.

The comparison of TEM images further reveals the evolution of particle morphology after cycling. The dark-field TEM images

in Fig. S4a† show the morphology of pristine SiO$_x$ and graphite. Combined with the elemental mapping (Fig. S4b and c†), SiO$_x$ and graphite particles coexist in the pristine samples. The corresponding selected area electron diffraction (SAED) further confirms the amorphous feature of SiO$_x$ (Fig. S4d†), and the clear polycrystalline rings of graphite reflects its great crystallinity (Fig. S4e†).[29] These results are consistent with the above-mentioned XRD data. The cycled SiOC using E1 and E2 was subject of dark-field TEM (Fig. 4g and j) and elemental mapping (Fig. 4h, i, k and l). The SiO$_x$ particles in E1 were broken and dispersed around the graphite particles probably because of the poor mechanical property of the SEI. In contrast, SiO$_x$ cycled in E2 still remains as the whole particle, in accordance with the results observed by SEM. In Fig. S5,† the graphite lamellae and flake structure can be clearly observed after a series of low-temperature tests.
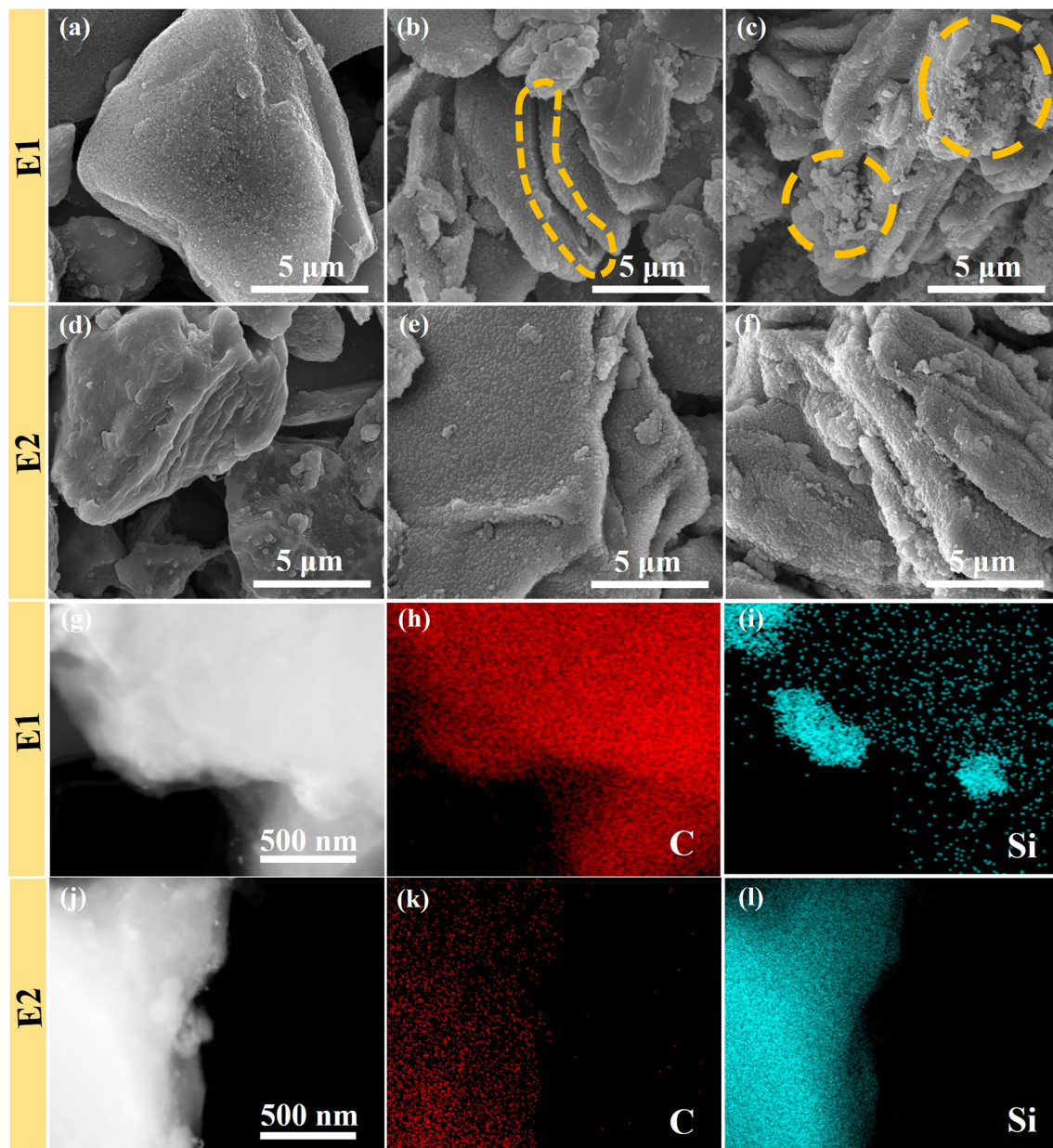
Fig. 4 SEM images of SiOC electrodes with E1 and E2 after different cycles: (a and d) 1st cycle at 0.1C, (b and e) 10th cycles at 0.1C, (c and f) after finishing all low-temperature tests; yellow circles specifically display the area of cracks. The dark-field TEM images of the electrodes with (g) E1 and (j) E2 electrolytes after finishing all tests at low temperatures and the corresponding elemental mappings of (h and k) C element and (i and l) Si element.

Comparison of XPS in Fig. 5 gives information about the change in chemical composition for the electrode surface during cycling for E1 and E2. Fig. 5a displays the surface substance containing carbon of pristine electrode. A distinct graphite peak at 283.8 eV was consistent with the XRD result and this peak disappeared after cycling and two new C 1s peaks were observed at 288.8 eV and 290.7 eV (Fig. 5d and g), suggesting the generation of species containing CO_3^{2-} and C–F on the electrode.[43] The F 1s spectrum of the cycled electrode can be divided into a dominant peak at 685.0 eV for LiF and a small peak at 687.4 eV for $Li_xPF_yO_z$. The intensity of LiF on the surface of SiOC in E2 is higher than that in E1 (Table S2†). The

formation of LiF has been well demonstrated to provide a minimum activation barrier to achieve the rapid diffusion of Li^+ ions[43–45] and to improve the flexibility of SEI.[46] In addition, it has been reported that increasing the LiF content in SEI is correlated with the improved electrochemical performance of cells, by lowering the impedance of the cell, and leads to better cycling performance.[47,48] Therefore, we propose that the EP co-solvent in E2 can promote the formation of LiF-rich SEI and improve the mass and/or charge transfer kinetics of SiOC anodes. In the Si 2p spectrum, two peaks of SiO_2 at 103.3 eV and Si at 99.7 eV are transformed into a weak broad peak at 101.9 eV, verifying the generation of Li_xSiO_y,[49] which can maintain the
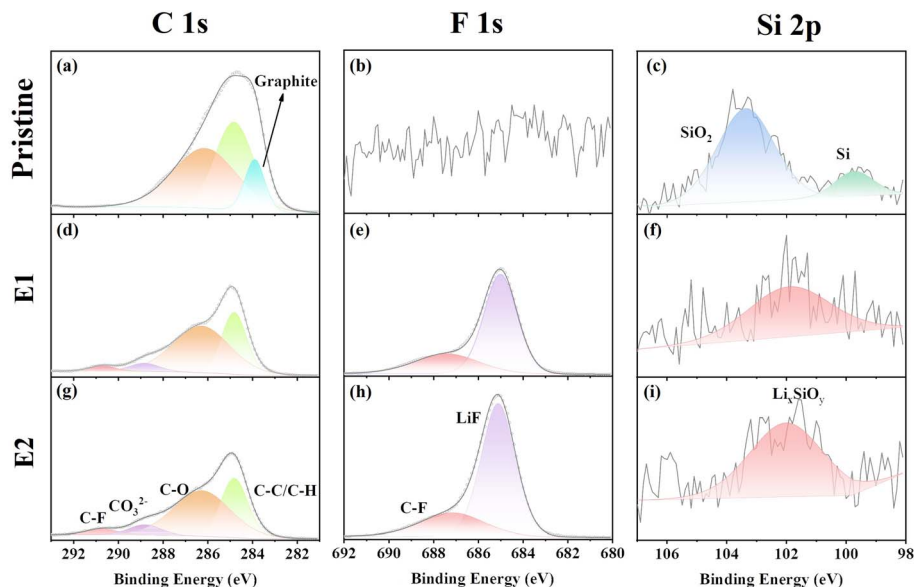
Fig. 5 Fitted XPS analysis (C 1s, F 1s, and Si 2p spectra) of (a–c) pristine electrode and electrodes with (d–f) E1 and (g–i) E2 cycled at low temperatures.

integrity of the electrode structure and improve the cycling performance.[50] The film-forming process and the variation in electrode are schematically summarized in Fig. S6,† which depicts that E2 possesses a better film-forming ability and such SEI shows ideal flexibility even at low temperatures. Thus, the expansion and cracking of SiO$_x$ particles are restrained effectively.

We also evaluated the feasibility of EP-based electrolyte E2 for SiOC‖LCO full cells (Fig. 6a) with a N/P ratio of 0.87, in comparison with E1. The full cell with E2 can achieve stable charge–discharge at −20 °C and 0.1C for 200 cycles, with the capacity retention of 94.08%, while the full cell using E1 has a retention ratio of 91.82% under the same low-temperature cycling conditions. Furthermore, the average capacity in E2 of
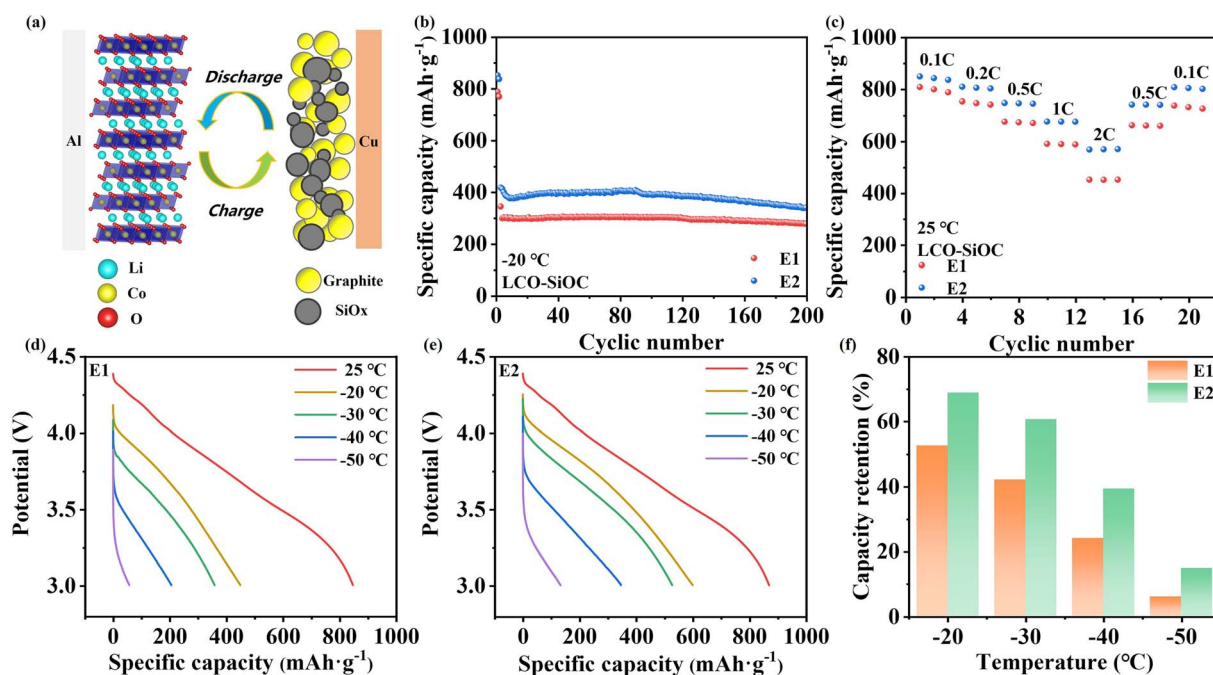

Fig. 6 (a) Schematic diagram of the SiOC‖LCO full cell. Comparison of electrochemical performance of the SiOC‖LCO full cell with E1 and E2 electrolytes: (b) cyclic performance at −20 °C and 0.1C; (c) rate performance at 25 °C; discharge curves at 0.1C and different temperatures of cells with (d) E1 and (e) E2, in which the cells were charged at 25 °C and 0.1C. (f) Comparison of capacity retention at different temperatures. Note: all the specific capacity results were calculated based on the weight of the anode active material.

385.86 mA h g^{-1} is about 28.45% higher than that in E1 of 300.40 mA h g^{-1} (Fig. 6b), demonstrating the positive effect of E2 on cycling capacity. The corresponding charge–discharge curves in Fig. S7a and b† and comparison of multiplier performance of the two full cells at −20 °C (Fig. S8†) also verify the superior performance of the full cell using E2 at low temperatures. Based on the mass of the SiOC anode material, full cells with E2 electrolyte possess discharge capacities (0.1C) of 600.51, 528.11, 346.62, and 132.75 mA h g^{-1} at −20, −30, −40, and −50 °C (Fig. 6e), respectively, about 33.41–132.81% higher than cells with E1, which have discharge capacities of 450.10, 359.31, 206.25, and 57.02 mA h g^{-1} at these temperatures (Fig. 6d). Comparison of the capacity retention of full cells (Fig. 6f) can also demonstrate the improvement effect of E2 at low temperatures, i.e., 68.85%, 60.66%, 39.34%, and 14.75% at −20, −30, −40, and −50 °C of E2, while 52.63%, 42.1%, 24.06%, and 6.01% of E1 at higher temperatures. In addition, the rate capability at 25 °C is shown in Fig. 6c. These results prove the feasibility of EP-based low-temperature electrolytes in full cells.

4. Conclusions

To develop low-temperature electrolytes for silicon-based anodes, we have designed an electrolyte E2 that contains linear carboxylic ester co-solvent EP, and compared with electrolyte E1 without any ester. The electrochemical performance of the SiO$_x$/graphite composite anode SiOC in the two electrolytes was examined, and SiOC with E2 showed better and excellent low-temperature performance and cycling stability at ambient temperature. At a temperature as low as −50 °C, a high capacity of 680.31 mA h g^{-1} was achieved, with an excellent capacity retention of 63.66% compared with that at 25 °C. The capacity retention reaches 97.02% after 100 cycles at 25 °C. It was demonstrated that the usage of E2 in SiOC‖LCO full cells guaranteed excellent cycling stability at −20 °C. As revealed by SEM, TEM and XPS characterizations, the LiF-rich SEI formed in E2 exhibits excellent mechanical properties and adaptability to the large volume change of SiO$_x$/graphite composite anodes at low temperatures.

Conflicts of interest

There are no conflicts to declare.

Acknowledgements

References

1 N. N. Yao, Y. Zhang, X. H. Rao, Z. Yang, K. Zheng, K. Swierczek and H. L. Zhao, *Int. J. Miner., Metall. Mater.*, 2022, **29**, 876–895.

2 J. Zhang, X. Zhang, Z. Hou, L. Zhang and C. Li, *J. Alloys Compd.*, 2019, **809**, 151798.

3 J. Wu, Y. Cao, H. Zhao, J. Mao and Z. Guo, *Carbon Energy*, 2019, **1**, 57–76.

4 H. Dong, J. Wang, H. Ding, F. Zong, P. Wang, R. Song, N. Zhang, X. Cui, X. Cui and S. Li, *Ionics*, 2022, **28**, 3057–3077.

5 P. Huang, B. Liu, J. Zhang, M. Liu and Z. Xie, *Ionics*, 2021, **27**, 1957–1966.

6 L. Xie, H. Liu, S. Lin, X. Yang, M. Qi, L. Zhu, Y. Guo and G. Guo, *RSC Adv.*, 2019, **9**, 11369–11376.

7 J. Wang, T. Xu, X. Huang, H. Li and T. Ma, *RSC Adv.*, 2016, **6**, 87778–87790.

8 N. Piao, X. Gao, H. Yang, Z. Guo, G. Hu, H.-M. Cheng and F. Li, *Etransportation*, 2022, **11**, 100145.

9 M. J. Piemas-Munoz, S. E. Trask, A. R. Dunlop, E. Lee and I. Bloom, *J. Power Sources*, 2020, **448**, 227080.

10 E. Markevich, G. Salitra and D. Aurbach, *J. Electrochem. Soc.*, 2016, **163**, A2407–A2412.

11 X. Liu, X. Sun, X. Shi, D. Song, H. Zhang, C. Li, K.-Y. Wang, C. Xiao, X. Liu and L. Zhang, *Chem. Eng. J.*, 2021, **421**, 127782.

12 T. Subburaj, W. Brevet, F. Farmakis, D. Tsiplakides, S. Balomenou, N. Strataki, C. Elmasides, B. Samaniego and M. Nestoridi, *Electrochim. Acta*, 2020, **354**, 136652.

13 B. Liu, B. Li and S. Guan, *Electrochem. Solid-State Lett.*, 2012, **15**, A77–A79.

14 S. S. Zhang, K. Xu and T. R. Jow, *J. Solid State Electrochem.*, 2003, **7**, 147–151.

15 D. Hubble, D. E. Brown, Y. Zhao, C. Fang, J. Lau, B. D. McCloskey and G. Liu, *Energy Environ. Sci.*, 2022, **15**, 550–578.

16 G. Zhu, K. Wen, W. Lv, X. Zhou, Y. Liang, F. Yang, Z. Chen, M. Zou, J. Li, Y. Zhang and W. He, *J. Power Sources*, 2015, **300**, 29–40.

17 Q. Li, G. Liu, H. Cheng, Q. Sun, J. Zhang and J. Ming, *Chem.–Eur. J.*, 2021, **27**, 15842–15865.

18 B. Nan, L. Chen, N. D. Rodrigo, O. Borodin, N. Piao, J. Xia, T. Pollard, S. Hou, J. Zhang, X. Ji, J. Xu, X. Zhang, L. Ma, X. He, S. Liu, H. Wan, E. Hu, W. Zhang, K. Xu, X.-Q. Yang, B. Lucht and C. Wang, *Angew. Chem., Int. Ed.*, 2022, **61**, e202205967.

19 M. C. Smart, B. L. Lucht, S. Dalavi, F. C. Krause and B. V. Ratnakumar, *J. Electrochem. Soc.*, 2012, **159**, A739–A751.

20 M. C. Smart, B. V. Ratnakumar and S. Surampudi, *J. Electrochem. Soc.*, 2002, **149**, A361–A370.

21 X. Dong, Z. Guo, Z. Guo, Y. Wang and Y. Xia, *Joule*, 2018, **2**, 902–913.

22 X. Dong, Y. Lin, P. Li, Y. Ma, J. Huang, D. Bin, Y. Wang, Y. Qi and Y. Xia, *Angew. Chem., Int. Ed.*, 2019, **58**, 5623–5627.

23 N. Zhang, T. Deng, S. Zhang, C. Wang, L. Chen, C. Wang and X. Fan, *Adv. Mater.*, 2022, **34**, 2107899.

24 S. Hong, J. Li, G.-c. Wang, Z.-a. Zhang and Y.-q. Lai, *Trans. Nonferrous Met. Soc. China*, 2015, **25**, 206–210.

25 M. C. Smart, B. V. Ratnakumar, K. B. Chin and L. D. Whitcanack, *J. Electrochem. Soc.*, 2010, **157**, A1361–A1374.

26 S. V. Sazhin, M. Y. Khimchenko, Y. N. Tritenichenko and H. S. Lim, *J. Power Sources*, 2000, **87**, 112–117.

27 X. Deng, S. Zhang, C. Chen, Q. Lan, G. Yang, T. Feng, H. Zhou, H. Wang, Z. Xu and M. Wu, *Electrochim. Acta*, 2022, **415**, 140268.

28 M. Xu, J. Ma, G. Niu, H. Yang, M. Sun, X. Zhao, T. Yang, L. Chen and C. Wang, *ACS Omega*, 2020, **5**, 16440–16447.

29 H. P. Zhou, B. Yang, Z. D. Zhang, H. Zhang, S. Zhang, T. T. Feng, Z. Q. Xu, J. Gao and M. Q. Wu, *Appl. Surf. Sci.*, 2022, **605**, 154627.

30 G. Zheng, Y. Xiang, L. Xu, H. Luo, B. Wang, Y. Liu, X. Han, W. Zhao, S. Chen, H. Chen, Q. Zhang, T. Zhu and Y. Yang, *Adv. Energy Mater.*, 2018, **8**, 1801718.

31 D. Gueon, D.-Y. Kang, J. S. Kim, T. Y. Kim, J. K. Lee and J. H. Moon, *J. Mater. Chem. A*, 2015, **3**, 23684–23689.

32 K. Xu, *Chem. Rev.*, 2014, **114**, 11503–11618.

33 X. Li, J. Liu, J. He, S. Qi, M. Wu, H. Wang, G. Jiang, J. Huang, D. Wu, F. Li and J. Ma, *Adv. Sci.*, 2022, **9**, 2201297.

34 Z. Yu, H. Wang, X. Kong, W. Huang, Y. Tsao, D. G. Mackanic, K. Wang, X. Wang, W. Huang, S. Choudhury, Y. Zheng, C. V. Amanchukwu, S. T. Hung, Y. Ma, E. G. Lomeli, J. Qin, Y. Cui and Z. Bao, *Nat. Energy*, 2020, **5**, 526–533.

35 J. Liu, P. Kopold, P. A. van Aken, J. Maier and Y. Yu, *Angew. Chem., Int. Ed.*, 2015, **54**, 9632–9636.

36 R. Miao, J. Zhu, S. Kang, J. Yang, J. Wang, J. Fu, M. Li and C. Shi, *Electrochim. Acta*, 2021, **384**, 138413.

37 J. Zhang, C. Zhang, Z. Liu, J. Zheng, Y. Zuo, C. Xue, C. Li and B. Cheng, *J. Power Sources*, 2017, **339**, 86–92.

38 Q. Xia, A. Xu, C. Huang, Y. Yan and S. Wu, *Chemelectrochem*, 2019, **6**, 4402–4410.

39 S. C. Jung, H.-J. Kim, J.-H. Kim and Y.-K. Han, *J. Phys. Chem. C*, 2016, **120**, 886–892.

40 B. Yin, L. Hao, T. Wei, C. Wang, B. Zhu, X. Li and Q. Yang, *Chem. Eng. J.*, 2022, **450**, 138224.

41 J. Zhang, W. Li, J. Wang, X. Pu, G. Zhang, S. Wang, N. Wang and X. Li, *Angew. Chem., Int. Ed. Engl.*, 2023, **62**, e202215654.

42 T. W. Kwon, J. W. Choi and A. Coskun, *Chem. Soc. Rev.*, 2018, **47**, 2145–2164.

43 Y. Yang, Z. Fang, Y. Yin, Y. Cao, Y. Wang, X. Dong and Y. Xia, *Angew. Chem., Int. Ed.*, 2022, **61**, e202213688.

44 Y. Lu, Z. Tu and L. A. Archer, *Nat. Mater.*, 2014, **13**, 961–969.

45 E. Markevich, G. Salitra and D. Aurbach, *ACS Energy Lett.*, 2017, **2**, 1337–1345.

46 H. Jia, L. Zou, P. Gao, X. Cao, W. Zhao, Y. He, M. H. Engelhard, S. D. Burton, H. Wang, X. Ren, Q. Li, R. Yi, X. Zhang, C. Wang, Z. Xu, X. Li, J.-G. Zhang and W. Xu, *Adv. Energy Mater.*, 2019, **9**, 1700784.

47 J. Fu, X. Ji, J. Chen, L. Chen, X. Fan, D. Mu and C. Wang, *Angew. Chem., Int. Ed.*, 2020, **59**, 22194–22201.

48 Y. Liu, X. Tao, Y. Wang, C. Jiang, C. Ma, O. Sheng, G. Lu and X. W. Lou, *Science*, 2022, **375**, 739–745.

49 M. Nie, D. P. Abraham, Y. Chen, A. Bose and B. L. Lucht, *J. Phys. Chem. C*, 2013, **117**, 13403–13412.

50 J. Zhang, P. Ma, X. Zhang, Z. Liu, J. Zheng, Y. Zuo, C. Xue, B. Cheng and C. Li, *Energy Technol.*, 2019, **7**, 1800800.